

Three-dimensional tuning of idiophone bar modes via finite element analysis^{a)}

Douglas Beaton^{b)} and Gary Scavone

Computational Acoustic Modeling Laboratory, Center for Interdisciplinary Research in Music Media and Technology, Schulich School of Music, McGill University, Montreal, Quebec, H3A 1E3, Canada

ABSTRACT:

The timbre of marimba and other idiophone bars can sometimes be polluted by untuned torsional modes, leading to substandard instruments or rejected materials. Makers have complained of problems with these untuned modes over a specific range of notes. Marimba, vibraphone, and similar idiophone bars are tuned by carving one side of the bar to bring up to three flexural modes into harmonic relationships. Torsional and other mode types are commonly left untuned. The relative frequency of these untuned modes with respect to the fundamental mode will vary along the keyboard. This paper investigates tuning both torsional and flexural modes simultaneously. This tuning is achieved using sophisticated carved geometries, and without employing concentrated masses or additional materials. Bars are modeled using three-dimensional finite elements. Geometry is defined by a large number of input parameters. Algorithms are implemented to identify bar modes automatically, eliminating the need for human intervention. Tuning is performed via a Newton-Raphson approach using the Moore-Penrose generalized matrix inverse to solve systems of tuning equations. This method is found to be effective at finding satisfactory bar geometries in proximity to initial conditions. Numerous example marimba and vibraphone bar models are provided, representing both typical and atypical modal tuning ratios. © 2021 Acoustical Society of America. <https://doi.org/10.1121/10.0005062>

(Received 29 December 2020; revised 28 April 2021; accepted 30 April 2021; published online 2 June 2021)

[Editor: Nicholas J. Giordano]

Pages: 3758–3768

I. INTRODUCTION

The bars of marimbas, vibraphones and similar bar percussion instruments are tuned by shaping their geometry. Bars are typically tuned by carving out a “cutaway” or “undercut” on the bottom of the bar, while maintaining a flat playing surface on top. A bar’s fundamental frequency will be tuned to its intended musical note. Some number of additional higher partials will also be tuned to harmonic ratios of the fundamental. Lower notes on marimbas and vibraphones will commonly have two additional partials tuned, while a single additional partial will be tuned for higher notes. The ratios of these tuned partial frequencies to the fundamental is most often set to 1:4:10 for marimbas and vibraphones while 1:3:6 can be observed in xylophones (Moore, 1970; Orduña-Bustamante, 1991).

The fundamental and tuned partials of these bars are produced by flexural modes of vibration with movement transverse to a bar’s playing surface. These modes are thus commonly termed “transverse modes” in the literature. Other modes types, including lateral-flexural, axial, and torsional modes, are not typically tuned. Figure 1 shows examples of these mode types for a bar with free-free boundary conditions, along with the naming scheme adopted in this work. While many of these modes will have a negligible

effect on a bar’s sound, makers have complained of certain torsional modes polluting bar timbre (Stevens, 2015) leading to reject bars and wasting valuable materials. These torsional modes can be excited when striking a bar away from its longitudinal axis of symmetry.

This paper investigates using a three-dimensional (3D) finite element (FE) model to tune torsional and/or lateral-flexural modes of aluminum or rosewood bars in addition to the commonly tuned transverse modes (termed “vertical modes” in this work). All modes are tuned only by varying geometry and without attaching any concentrated mass or reinforcing materials. Sections of uniform thickness are maintained at the ends of each bar to be consistent with typical professional instruments and to provide locations for support cable holes.

II. BACKGROUND

Numerous studies of idiophone bars are available in the literature. These studies include finite difference models (Chaigne and Doutaut, 1997; Orduña-Bustamante, 1991), 1D FE models with beam elements (Henrique and Antunes, 2003; Petrolito and Legge, 1997, 2005) to 3D FE models with continuum elements (Bestle *et al.*, 2017; Bork *et al.*, 1999; Bretos *et al.*, 1999). Topics covered include optimizing bar geometry (Henrique and Antunes, 2003; Kirkland and Moradi, 2016; Petrolito and Legge, 1997, 2005), comparing FE models with experimental measurements (Bestle *et al.*, 2017; Bork *et al.*, 1999; Bretos *et al.*, 1997, 1999),

^{a)}This paper is part of a special issue on Modeling of Musical Instruments.

^{b)}Electronic mail: douglas.beaton@mail.mcgill.ca, ORCID: 0000-0002-5517-3801.

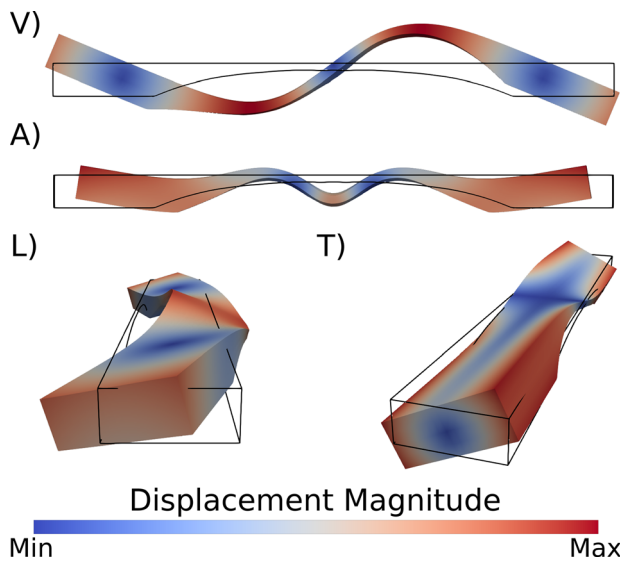


FIG. 1. (Color online) Vibration mode types and labels considered in this work. Undeformed bar geometry is outlined in black. Free-free boundary conditions are employed. Mode types: (V)—vertical-flexural mode, (A)—axial mode, (L)—lateral-flexural mode, (T)—torsional mode. Note that the bar cutaway in this example results in coupling between deformation types. Vertical deformation is present in the axial mode, while torsional deformation occurs in the lateral-flexural mode.

modeling for fabrication via CNC mill (Kirkland and Moradi, 2016), and sequential fabrication and model updating for wooden bars (Mingming, 2011).

Various methods of shape optimization have been employed in the literature to tune bar cutaways. Henrique and Antunes (2003) applied both simulated annealing and sequential quadratic programming (SQP) to tune the modes of 1D vibraphone bar models by minimizing an error function. Petrolito and Legge (2005) also employed SQP in tuning 1D aluminum bars, though their approach set modal frequencies as constraints and sought to optimize bar volume and/or smoothness. Kirkland and Moradi (2016) adopted that same approach to tune 3D models of vibraphone bars while optimizing bar volume. Soares et al. (2021) used an evolutionary optimization algorithm to tune 1D bars with simplified undercuts, using a combination of mode tuning, bar volume and/or smoothness objectives.

The 3D idiophone bar models cited above are nominally three-dimensional in that, at any given point along their length, bar thickness is uniform across their width. Put differently, each of the 3D bars previously considered is essentially a 2D model extruded into the third dimension.

Previous work by the authors (Beaton and Scavone, 2019) investigated using 3D finite element models to tune vertical-flexural bar modes. Bar cutaway geometry in that work was defined either by interpolating between defined cross-sections at specified positions or interpolating over a grid of thickness control points. Cross-sectional interpolation required a small number of inputs and was coupled with Newton-Raphson iterations to tune an equal number of vertical-flexural modes. This approach led to smooth bar geometries but had limited ability to affect torsional

behavior. Surface interpolation required a large number of inputs and was coupled with genetic algorithms to tune vertical-flexural modes. That approach yielded bar geometries that were in tune, though not smooth. Alternative genetic algorithm formulations could certainly lead to bars that are both smooth and in tune, though a large number of model runs would likely be required.

This study furthers these previous efforts by using 3D finite element analysis to tune bar torsional modes. Cutaway geometries are defined using a surface interpolation approach with enforced symmetry (see Sec. III). This approach allows for greater flexibility than cross-sectional interpolation, while maintaining a manageable number of inputs. While studies cited above employed optimization methods to tune bar geometry, in this work the tuning problem is formulated as solving a system of nonlinear equations. Petrolito and Legge (2005) considered this formulation, though they expected that the number of input variables must equal the number of tuned modes and thus would “not allow sufficient latitude for describing the shape of the structure.” As will be shown, this formulation can be employed while allowing the number of input variables to exceed the number of tuned modes. To accommodate the additional input variables, models are tuned using a Newton-Raphson approach adapted to solve underdetermined systems of tuning equations (see Sec. III A). This method provides the advantages of gradient-based solving while determining both search direction and step size simultaneously, rather than sequentially, as is sometimes required with other methods. The resulting analyses demonstrate the feasibility of tuning both flexural and torsional bar modes solely via changes to cutaway geometry.

III. METHODOLOGY

Bar cutaway geometry was defined by interpolating thickness over a 2D grid of control points. This same method was employed in previous work by the authors (Beaton and Scavone, 2019). Figure 2 shows an example layout of control points. To enforce cutaway symmetry, and reduce the number of input variables, some control points were defined by mirroring others. The control points in group 1 of Fig. 2 were set as inputs, with group 2 defined by mirroring group 1. Group 3 control points were defined by mirroring groups 1 and 2. This doubly mirrored approach served to enforce two planes of cutaway symmetry and was termed a *quarter-surface* definition. Several analyses were

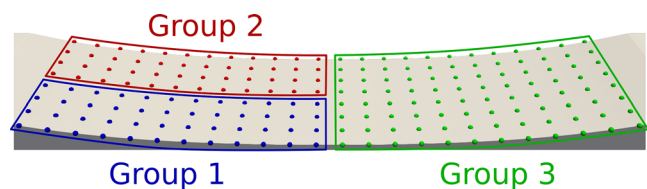


FIG. 2. (Color online) Detailed view of example control points and groups used to define bar cutaway geometry. Typically, group 1 points were used as design inputs while points in groups 2 and 3 were defined by mirroring. Sections of uniform thickness at each end of the bar are not shown.

TABLE I. Modeled bar dimensions based on measurements of an Adams marimba and Yamaha vibraphone. L and W give bar length and width, respectively. T_{max} indicates the maximum thickness of the indicated bar, as occurs in the uniform segments at each end. T_{min} gives the minimum observed bar thickness over the whole instrument.

Instrument	Note	Bar dimensions [mm]			
		L	W	T_{max}	T_{min}
Marimba	F3	406	58	24	6
Vibraphone	C4	333	57	13	5

also run using a *half-surface* definition, in which groups 1 and 2 of Fig. 2 were inputs, with group 3 again mirrored. Given the same doubly symmetric initial geometry, these half-surface models yielded results essentially identical to the quarter-surface models. With equivalent results and lower computational costs, quarter-surface definition was adopted for all analyses in this work.

Marimba and vibraphone bars of notes F3 and C4 were selected for analysis. Marimba bars were modeled as rosewood while vibraphone bars were defined as aluminum. Table I outlines modeled bar dimensions while Table II details the material properties used. Bar dimensions were based on measured values from an Adams marimba and Yamaha vibraphone. Rosewood material properties were adopted from Bork *et al.* (1999). Aluminum properties were based on the popular 6061 alloy (Battelle Memorial Institute, 2020).

A. Tuning approach

The bar tuning problem is formulated as

$$\text{set } \mathbf{g}(\mathbf{x}) = \mathbf{0}, \quad T_{min} \leq x_n \leq T_{max}, \quad n \in [1, N], \quad (1)$$

where $\mathbf{g}(\mathbf{x})$ is a vector of tuning functions, \mathbf{x} is a vector of bar thickness values at the control points in Fig. 2, T_{min} and T_{max} are thickness limits defined in Table I, and n is an index variable up to the total number of control points, N . A single tuning function in the $\mathbf{g}(\mathbf{x})$ vector takes the form

$$g_k(\mathbf{x}) = \frac{f_{\text{model},k}(\mathbf{x}) - f_{\text{target},k}}{f_{\text{target},k}}, \quad (2)$$

TABLE II Bar material properties with: density, ρ , Young's modulus, E , Poisson's ratio, ν , and shear modulus, G . Rosewood properties are adopted from the literature (Bork *et al.*, 1999). Aluminum properties are from the standard 6061 alloy (Battelle Memorial Institute, 2020).

Material	ρ [kg/m ³]	E [GPa]	ν	G [GPa]
Aluminum	2700	68.9	0.33	25.9
Rosewood	1080			
x-axis		23.0		
y-axis		2.3		
z-axis		1.15		
xy-plane			0.30	3.0
yz-plane			0.60	1.0
xz-plane			0.45	3.0

where $g_k(\mathbf{x})$ is the k th tuning function, $f_{\text{model},k}(\mathbf{x})$ the modeled frequency of the k th tuned mode, and $f_{\text{target},k}$ the target frequency for that mode. With this formulation each tuning function, $g_k(\mathbf{x})$, represents the normalized error between the modeled frequency of the k th tuned mode, for a given input vector \mathbf{x} , and the target frequency for that mode. Thus when $g_k(\mathbf{x}) = 0$ the k th tuned mode is perfectly in tune. In practice a tolerance is employed such that if $|g_k(\mathbf{x})| \leq 1 \text{ cent } \forall k$, Eq. (1) is considered solved.

Generally each tuning function, $g_k(\mathbf{x})$, will be nonlinear as the modal frequencies in $f_{\text{model},k}(\mathbf{x})$ will be nonlinear functions of the control point thickness values in \mathbf{x} . Let K be the total number of tuned modes, while N is the total number of control points in Fig. 2. For all models considered in this work $K \leq 6$ and $N = 48$, so $K \ll N$. Equation (1) thus describes an underdetermined nonlinear system (Macconi *et al.*, 2009). The roots of this system represent bar geometries that tune the specified modes to their desired frequencies.

Equation (1) was solved by applying the Newton-Raphson method to an underdetermined system using a generalized inverse Jacobian matrix. Recall that roots of nonlinear scalar functions can be found using the familiar formula for Newton-Raphson iteration

$$y_{i+1} = y_i - \frac{h(y_i)}{h'(y_i)}, \quad (3)$$

where y_i is the estimated root of nonlinear function $h(y)$ at the i th iteration, and $h'(y)$ the first derivative of $h(y)$. Equation (3) is applied iteratively from a given starting point, y_0 , to find a root of the nonlinear function. This approach can be expanded to vector inputs and functions as

$$\mathbf{y}_{i+1} = \mathbf{y}_i - \mathbf{J}^{-1}(\mathbf{y}_i)\mathbf{p}(\mathbf{y}_i), \quad (4)$$

where vector \mathbf{y}_i is the estimated root of vector function $\mathbf{p}(\mathbf{y})$ at the i th iteration, and $\mathbf{J}(\mathbf{y})$ is the Jacobian matrix of partial derivatives of $\mathbf{p}(\mathbf{y})$ with respect to the components of \mathbf{y} . Applying Eq. (4) requires inverting $\mathbf{J}(\mathbf{y})$ (or rearranging and solving a system of equations), thus the number of terms in $\mathbf{p}(\mathbf{y})$ must equal the number of inputs in \mathbf{y} to ensure $\mathbf{J}(\mathbf{y})$ will be a square matrix.

With K tuned modes, function $\mathbf{g}(\mathbf{x})$ in Eq. (1) will be a column vector of length K . Using N control point thickness values as inputs, \mathbf{x} will be a column vector of length N . Thus the Jacobian matrix $\mathbf{J}(\mathbf{x})$ containing partial derivatives of $\mathbf{g}(\mathbf{x})$ will have dimensions $K \times N$. In such a case, Eq. (1) can be solved by modifying Eq. (4) to

$$\mathbf{x}_{i+1} = \mathbf{x}_i - \mathbf{J}^+(\mathbf{x}_i)\mathbf{g}(\mathbf{x}_i), \quad (5)$$

where $\mathbf{J}^+(\mathbf{x})$ is the Moore-Penrose inverse (Ben-Israel, 2002; Penrose, 1955) (sometimes called the *pseudoinverse*) of $\mathbf{J}(\mathbf{x})$, which now contains the partial derivatives of $\mathbf{g}(\mathbf{x})$. Note that Eq. (5) takes the same form as the Gauss-Newton method for solving nonlinear least squares problems. When

applied to solve an underdetermined linear system the Moore-Penrose inverse will produce the solution with minimum norm (Ben-Israel and Greville, 2003). Applying the Moore-Penrose inverse in Eq. (5) thus produces the estimated solution, \mathbf{x}_{i+1} , of Eq. (1) which lies nearest the current estimate \mathbf{x}_i . Any values in \mathbf{x}_{i+1} lying outside the thickness limits in Table I are replaced with the corresponding limit value. Convergence will slow as values in \mathbf{x}_{i+1} reach one of the thickness limits. To mitigate this effect, Eq. (5) is modified as

$$\mathbf{x}_{i+1} = \mathbf{x}_i - [\mathbf{J}(\mathbf{x}_i)\mathbf{D}(\mathbf{x}_i)]^+ \mathbf{g}(\mathbf{x}_i), \quad (6)$$

where $\mathbf{D}(\mathbf{x})$ is a diagonal binary matrix. This matrix serves to remove the effects of any inputs that have hit a limit and would be pushed beyond that limit if included in the calculation. The matrix is defined as

$$\mathbf{D}(\mathbf{x}) = \text{diag}[b_1(\mathbf{x}), b_2(\mathbf{x}), \dots, b_N(\mathbf{x})], \quad (7)$$

$$b_n(\mathbf{x}) = \begin{cases} 0 & \text{if } [\mathbf{J}^+(\mathbf{x})\mathbf{g}(\mathbf{x})]_n > 0, x_n = T_{min}, \\ & \text{or } [\mathbf{J}^+(\mathbf{x})\mathbf{g}(\mathbf{x})]_n < 0, x_n = T_{max}, \\ 1 & \text{otherwise.} \end{cases} \quad (8)$$

Using this formulation, Eq. (6) is applied in the same iterative manner as Eq. (4) to find the roots of $\mathbf{g}(\mathbf{x})$. Examples of other approaches to solve Eq. (1) can be found in the literature, including Levenberg-Marquardt-type methods (Kanzow *et al.*, 2004), and methods also employing the Moore-Penrose inverse (Macconi *et al.*, 2009). The method used here is selected for its relative simplicity and emphasis on finding solutions similar to initial geometry.

B. Finite element model

Figure 3 shows an example bar model from this work. All models considered are comprised of either 8-node or 20-node hexahedral continuum elements arranged in a structured finite element mesh. The numbers of elements along the bar’s length, width and thickness directions were defined and adjusted parametrically. Free-free boundary conditions were employed in the calculation of mode shapes and frequencies. The calculated results are natural frequencies without consideration of damping. Analyses were performed using finite element software written by the first author and

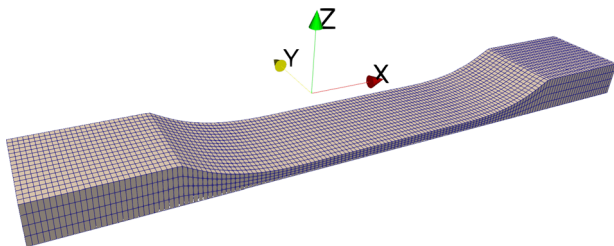


FIG. 3. (Color online) Initial (untuned) geometry of an F3 marimba bar with arbitrary “carved” cutaway shape. Model coordinate axes align with bar dimensions as: x axis \rightarrow length, y axis \rightarrow width, z -axis \rightarrow thickness.

verified against the open-source program CALCULIX (Dhondt, 2019). The Jacobian matrix of Eq. (5) was populated in a semi-analytical manner. Nodal coordinate derivatives with respect to input variables were approximated using finite differences. From there, objective function derivatives were computed analytically using established methods to compute the required eigenvalue sensitivities (Wang *et al.*, 1985). Bar cutaway thickness was limited to the range of values shown in Table I. These limits were based on measurements of existing instruments, recognizing a need for structural integrity. Evaluation of bar strength or fatigue when subjected to mallet strikes was not considered in this work.

IV. MODE IDENTIFICATION

An important and sometimes challenging aspect of this work was automatically identifying the 3D mode shapes. Finite element solvers produce modes ordered by frequency, with no indication of mode type (see Fig. 1). Over the course of bar tuning it is common for modal frequencies to change sufficiently to reorder the modes. For this reason, the program cannot be instructed to tune, for example, the first, third and fifth modes of the finite element model, as the modes of interest may not always appear in these positions. It is desirable that the tuning algorithms run unsupervised, without any need for the analyst to identify modes manually. For this reason, functions were implemented to identify modes automatically, without the need of human intervention.

This section uses the coordinate system shown in Fig. 3 when discussing bar mode shapes and deformations. Here, and throughout the paper, modes are named using the mode type letter abbreviation from Fig. 1, along with the number corresponding to that mode type. Thus, the third vertical mode is labeled “mode V3”; the first torsional mode is “mode T1” and so on. The overall ordering of modes is inconsequential, provided the number of modes calculated is large enough to capture those of interest.

A. Shape recognition

While the popular modal assurance criterion (discussed in Sec. IV B) is often applied to identify modes, it can do so only by comparison with a set of reference modes. It was preferable here to identify modes based solely on their displaced shapes. This allowed the tuning algorithm to execute with any geometry that is generally bar-shaped, regardless of outer dimensions, mesh or material. With the mode types shown in Fig. 1 solely of interest, an algorithm was implemented to identify modes by considering nodal displacements.

It is important to note here that this algorithm performs well on flat bars but can break down for bars with large cutaways. In such cases, coupling between deformation types is often observed. For example, as is shown in Fig. 1, longitudinal modes can include significant vertical displacements;

lateral-flexural modes can include torsional displacements. These cases are discussed in subsequent sections.

1. Axial modes

Over the frequency ranges considered in this work, only the first axial mode, with primary deformation along the bar's longitudinal axis, appeared. Thus, this mode was simple to identify. If the maximum absolute nodal displacement in the x-direction is larger than the maximum absolute displacements in the y- and z-directions, the mode is identified as axial.

2. Flexural modes

Flexural modes were identified by locating and assessing areas with low displacement magnitude (i.e., the norm of the three displacement components); these are the dark blue areas shown in Fig. 4 and throughout the paper. First, all nodes with displacement magnitude below a specified threshold were marked (pink dots, Fig. 4). These nodes were then separated into contiguous groups, based on element connectivity. Then, a line of best fit was calculated for each group (green lines, Fig. 4). Identification of flexural modes was based on the number and orientation of these lines. Two or more groups, each with a best-fit line parallel to the y axis indicates a vertical-flexural mode. Similarly, two or more groups, all with best-fit lines parallel to the z-axis indicates a lateral-flexural mode. For flexural modes, the mode number (e.g., third vertical mode, second lateral mode) is one less than the number of low-displacement groups.

3. Torsional modes

For flat and near-flat bars, over the frequency ranges considered, it was possible to identify torsional modes largely via process of elimination. After ruling out axial and flexural modes, any remaining modes were identified as torsional. For bars with significant cutaways, where torsional deformation may be present in lateral modes, a check was performed on the rotation of bar ends. If they were found to rotate to a greater extent about the z-axis than the x axis, the mode was instead labelled as lateral-flexural. This method of identifying torsional modes by process of elimination was

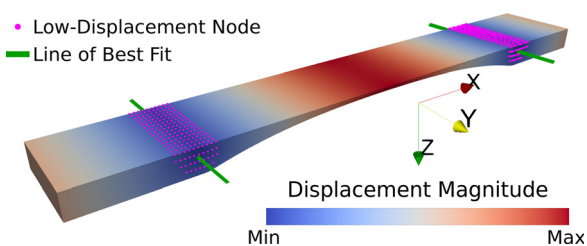


FIG. 4. (Color online) example of identifying modes based on shape recognition. Nodes highlighted in pink were identified as having low displacement magnitude. Lines of best fit for each node group (including interior nodes, not shown) are plotted in green. The bar's color map indicates displacement magnitude for the first mode of an aluminum C2 bar with initial carved geometry. Shape recognition identifies this as mode V1.

feasible for this work as other mode types, outlined below, appeared only in frequency ranges well above any modes that were tuned.

4. Modes not considered

Several mode types not considered above occur well beyond the range of frequencies relevant to bar tuning. These include axial modes along the y- and z-axes, flexural modes in the y-z plane, and torsional modes about the y- or z-axes.

B. Modal assurance criterion

The method of identifying modes via shape recognition proved reliable for bars of uniform thickness or with simple, modest undercuts. However, this method could run into trouble when faced with complex cutaway geometry or deep undercuts producing significant coupled deformation, particularly in lateral modes. To avoid unidentified or misidentified modes interrupting tuning iterations, the previously described shape identification was employed in identifying modes for the initial geometry (i.e., for the 0th iteration), and the popular modal assurance criterion (MAC) (Allemang, 2003) was applied to identify modes in subsequent iterations. In each case, modes identified in the previous iteration were used as reference modes. This approach produced generally satisfactory results, with a few important exceptions detailed below.

1. Degenerate modes

Whenever two modes in a bar model were very close in frequency the possibility of observing degenerate modes occurred. The mode shape of one or both degenerate modes will look like a weighted combination of the two modes with similar frequencies. Identification by automated shape recognition is not feasible in such a scenario and is frequently even difficult for an analyst to perform manually. The MAC also struggles in such cases as there will be rows and columns in the MAC matrix with two similar values, thus producing ambiguity.

Degenerate modes were observed in this work either when tuning two different modes to have the same frequency, or when iterative geometry changes would cause modes to reorder, producing degenerate modes in an intermediate step. In this second case, degenerate modes could appear during the tuning process even if they would not be expected with the final geometry.

When degenerate modes were encountered, a third identification approach was applied which maps the current geometry back to a geometry with known modes. This approach is outlined below.

2. Similar modes

The coupling of lateral and torsional deformations produced by deep undercuts can yield modes with incredibly similar shapes. Figure 5 shows one such case. The modes

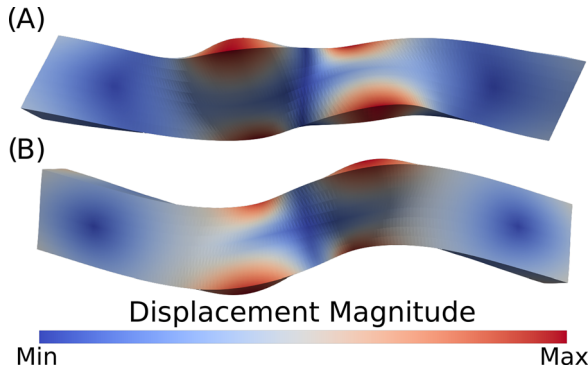


FIG. 5. (Color online) Top view of mode shapes that are similar without being degenerate. Results shown are from an Adams C3 bar model tuned to the typical 1:4:10 vertical mode ratios. Coupling between lateral and torsional deformations make it virtually impossible to identify either mode without additional information. (A) Mode L2, $f=2260$ Hz. (B) Mode T3, $f=2759$ Hz.

displayed have nearly indistinguishable shapes, while their frequencies differ by a full 22%. In this and similar cases, using MAC for mode identification between iterations can result in ambiguous results even in the absence of degenerate modes. Such cases are, however, easily handled using the same approach employed to identify degenerate modes, as outlined in Sec. IV C.

C. Mapping models to geometry with known modes

In cases where degenerate modes were encountered a third, robust yet labor intensive mode identification approach was employed. In this method, the current geometry, with degenerate modes, is mapped to a (typically simpler) reference model with known modes. A mapping variable, m , is defined to compute input vectors for intermediate models between the reference model and the current model. These intermediate input vectors are calculated as

$$\mathbf{x}_{\text{int}} = \mathbf{x}_{\text{ref}} + m(\mathbf{x}_{\text{deg}} - \mathbf{x}_{\text{ref}}), \quad m \in [0, 1], \quad (9)$$

where \mathbf{x}_{int} is the intermediate model input vector, \mathbf{x}_{ref} is the reference model input vector, m is the mapping variable, and \mathbf{x}_{deg} is the degenerate model input vector. From here the method works by using the known modes at $m=0$ to identify modes in models with progressively larger values of m using MAC. The degenerate modes can then be identified in one of two ways. Both options involve generating and evaluating intermediate models with values of m progressively closer to 1. MAC is used to identify modes in the intermediate models, using the model with the next-highest value of m as reference (beginning with the known model at $m=0$). In the first option, this process continues with progressively larger values of m until an intermediate model is produced that enables identifying the degenerate modes (at $m=1$) using MAC.

If identifying the degenerate modes in this manner using MAC proves problematic, an alternative is to generate and evaluate enough intermediate models to enable approximating the frequency of a given mode (e.g., mode V3) as a

function of m . These functions can then be used to predict the frequency of a given mode type at $m=1$. Additional intermediate models are generated until the resulting frequency predictions align with the degenerate mode frequencies sufficiently well to identify the modes.

V. RESULTS AND DISCUSSION

Figure 6 shows the resulting geometry for a rosewood bar model tuned to frequency ratios of 1:4:10:2:8:6 for modes V1, V2, V3, T1, T2, and L1, respectively. Figure 7 plots the tuned mode shapes for this bar.

This model exhibits several features appearing in other models as discussed below. Near each end of the cutaway, material is concentrated along the bar’s center while the edges are thin by comparison, creating a sort of central “spine.” These spines, and the thinner areas adjacent them, reduce torsional and lateral bending stiffness locally, lowering the frequency ratios of modes T1, T2, and L1 compared to their untuned state. This effect is evident in Fig. 7 as modes T1 and T2 show significant change in twist angle near these spines. At the bar’s midpoint material is distributed near the edges of the bar away from its center, having the opposite effect of increasing the bar’s torsional and lateral bending stiffness in these areas.

Average thickness across the bar’s width shows significant change at two positions: a noticeable step in the spine thickness at about a quarter of the cutaway length, and at each end of the thickened edges along the bar’s midpoint. These features clearly affect mode V3 as Fig. 7 shows concentrations of curvature in this mode at each of these locations.

Figure 8 shows a progression of submodels. Each submodel is the product of a separate analysis with a different set of modes tuned. Model 1(a) tunes a single mode only. Model 1(b) tunes the same mode as model 1(a), and one more. Each subsequent submodel tunes the same modes as the previous one, plus one additional mode. The target modal frequency ratios are outlined in Table III. Model 1(f), the final submodel in Fig. 8, also appears in Fig. 6, while model 1(e) is shown again in Fig. 9.

Also, included in Fig. 8 are frequency ratios for six modes in each submodel, some of which are left untuned. Open circle markers indicate tuned modes while all other markers represent modes left untuned in the corresponding submodel. Models 1(a), 1(b), and 1(c) are remarkably similar, with little deviation from the initial geometry in Fig. 3. This is unsurprising as these models progressively tune modes V1, V2, and V3 to the standard 1:4:10 ratios. The



FIG. 6. (Color online) Tuned geometry of model 1(f), a rosewood F3 bar tuned to modal frequency ratios: V1-1, V2-4, V3-10, T1-2, T2-8, L1-6.

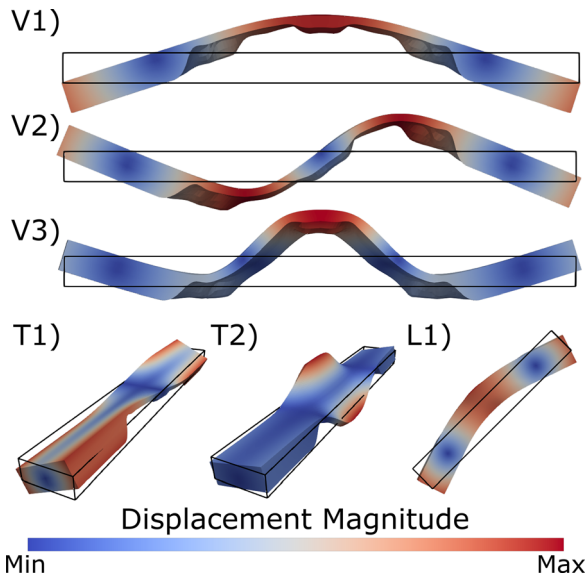


FIG. 7. (Color online) Tuned mode shapes of model 1(f), a rosewood F3 bar model tuned to frequency ratios: V1-1, V2-4, V3-10, T1-2, T2-8, L1-6. The undeformed bar position is shown as a black outline of the outer bar dimensions (cutaway omitted).

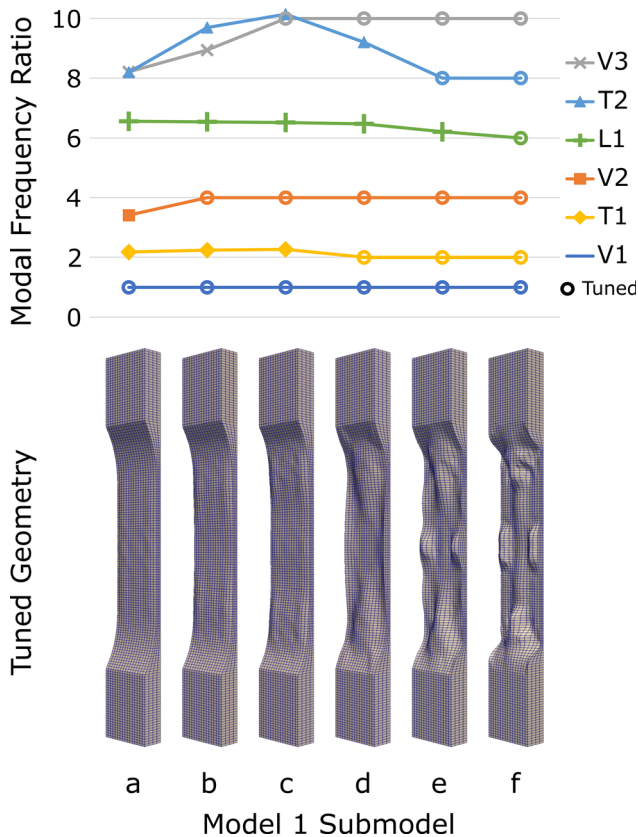


FIG. 8. (Color online) Geometry and modal frequency ratios for all model 1 submodels. Model 1(a) begins by tuning only Mode V1. Each successive model tunes one additional mode until modes V1, V2, V3, T1, T2, and L1 are all tuned in model 1(f). Plotted above is the progression of frequency ratios for the six modes over each submodel. Circle markers indicate a mode that is tuned in that submodel. All other markers represent untuned modes.

TABLE III Summary of example model input parameters.

Material	Note	Target tuning ratios						Initial geometry	Model No.
		V1	V2	V3	T1	T2	L1		
Rosewood	F3	1	—	—	—	—	—	Carved	1(a)
		1	4	—	—	—	—	Carved	1(b)
		1	4	10	—	—	—	Carved	1(c)
		1	4	10	2	—	—	Carved	1(d)
		1	4	10	2	8	—	Carved	1(e)
		1	4	10	2	8	6	Carved	1(f)
		1	4	10	—	11	—	Carved	2
		1	4	8	2	8	—	Carved	3
		1	5	9	3	7	—	Carved	4
		1	4	10	2	10	6	Carved	5
Aluminum	C4	1	3	9	—	7	—	Carved	7
		1	4	8	3	10	—	Carved	8
		1	4	10	3	12	8	Carved	9
		1	5	11	—	—	—	Carved	10
		—	—	—	—	—	—	Flat	6(b)
		—	—	—	—	—	—	Flat	6(b)

frequency ratios of modes T2 and V3 are very close in model 1(c), indicating an increased risk of timbral issues for such a bar. This demonstrates the potential problem when tuning vertical bending modes in the standard fashion while leaving torsional modes untuned.

More interesting geometry begins to appear in model 1(d), which adds mode T1 to the set of tuned modes. The spines discussed previously first appear in this submodel and become more pronounced in models 1(e) and 1(f). Some edge thickening is also apparent in model 1(d), becoming more noticeable in model 1(e), and more concentrated in model 1(f).

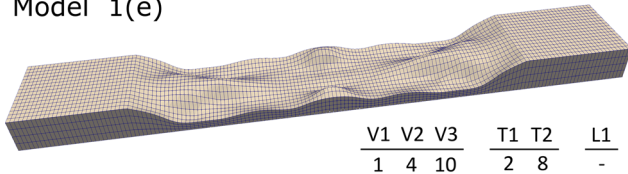
Table III outlines input parameters for all example models considered in this work. All models were run using quarter-surface definition with a 4×12 grid of control points, as shown in Fig. 2. Convergence was defined as having all tuned modes within one cent of their respective target values. Marimba bar examples with rosewood material properties are shown in Figs. 9 and 10. Vibraphone bar models with aluminum material properties are provided in Fig. 11. Bar outer dimensions are detailed in Table I.

Results will be referenced by model number in the discussion below. See Table III and Figs. 9–11 for info and resulting bar shapes for each model.

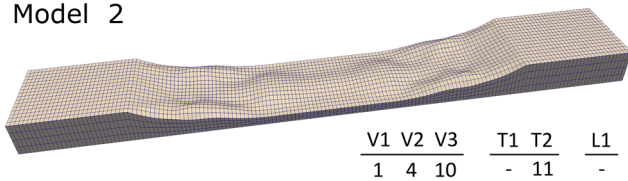
A. Geometry variability

The tuned bar shapes in Figs. 9–11 are quite interesting and show great variability in geometry. They also range in complexity. Model 10, which tunes only vertical modes, looks very similar to a commercial vibraphone bar while models 2 and 6(a) show only small deviations from typical marimba bar geometry. Other results, like models 3, 4, 6(b), or 7 are very different from any bar seen on a professionally made instrument today.

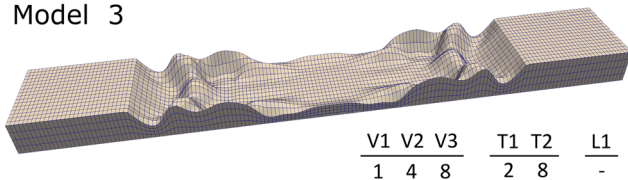
Model 1(e)



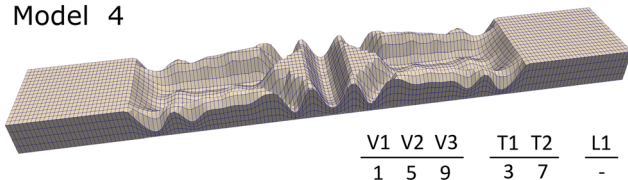
Model 2



Model 3



Model 4



Model 5

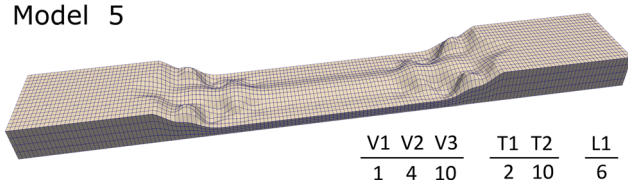
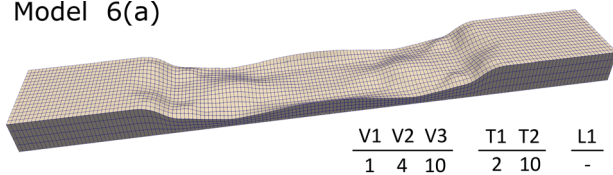


FIG. 9. (Color online) Tuned rosewood bar geometries for note F3. Ratios of modal frequencies to the fundamental are indicated for each bar; “-” indicates a mode left untuned. Model numbers are outlined in Table III.

B. Initial geometry

Models 6(a) and 6(b) in Fig. 10 demonstrate the importance of initial geometry selection. These models are each tuned to have the same frequency ratios but have very different geometries. Model 6(a) was initiated with the carved geometry shown in Fig. 3. Model 6(b) began with a flat bar

Model 6(a)



Model 6(b)

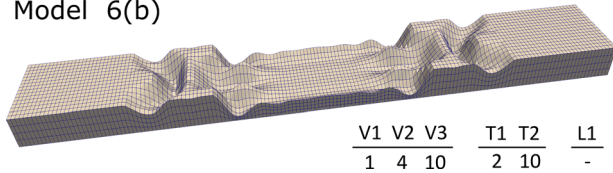
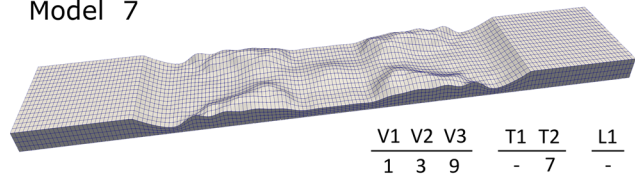
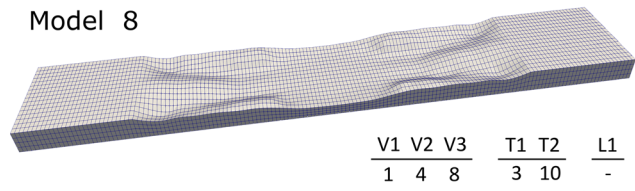


FIG. 10. (Color online) Tuned rosewood bar results for note F3. Ratios of modal frequencies to the fundamental are indicated for each bar; “-” indicates a mode left untuned. Model numbers and initial geometries are outlined in Table III. Though tuned to the same frequency ratios these models used different initial geometries (see Table III).

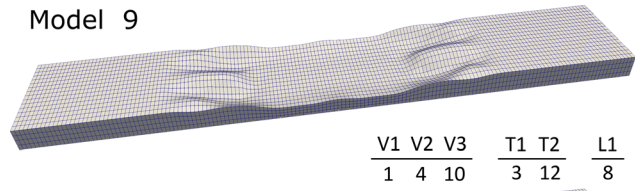
Model 7



Model 8



Model 9



Model 10

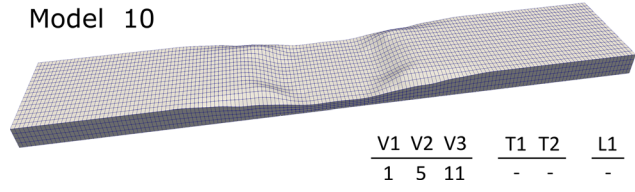


FIG. 11. (Color online) Tuned aluminum bar geometries for note C4. Ratios of modal frequencies to the fundamental are indicated for each bar; “-” indicates a mode left untuned. Model numbers are outlined in Table III.

of uniform thickness. These results demonstrate how each iteration of the tuning algorithm searches for the acceptable geometry nearest the current geometry for that iteration. The effects on final bar geometries are evident in Fig. 10, as model 6(a) is relatively smooth, having started from an initial geometry with a smooth cutaway. By contrast, the cutaway of model 6(b) includes several areas with maximum allowable thickness, reflecting the fact that this tuning run began with a uniform bar of maximum allowable thickness. When applying this tuning method, the analyst should therefore select a desirable bar geometry as starting point.

C. Hinge segments

Models 3 and 4 include thin cutaway segments concentrated over short lengths. These thin segments have the effect of concentrating mode shape curvature in local zones, thus behaving like a sort of hinge. The positions of these hinges determine which mode(s) they will affect. In model 4 a hinge near the midpoint along the bar’s length will serve to lower modes V1 and V3, while having a minimal effect on mode V2. This is reflected in the tuning ratios of model 4, where the tuning of mode V2 is increased to five times the fundamental—higher than is typically seen. Model 3 includes locally thin areas near the ends of the cutaway which curve slightly across the bar’s width. The locations of these hinge areas will serve to concentrate curvature in mode V3, thereby reducing its frequency ratio to the value of eight seen in this model. Model 7 includes similar, more elongated hinge areas at the ends of its cutaway. These

elongated hinges result in lowered frequency ratios for modes V2 and V3, which are tuned below their typical values in this model.

Interestingly, model 4 also displays two sets of angled hinge segments on either side of the central hinge at the bar's midpoint. These angled hinges have the greatest effect on mode T2, lowering its frequency ratio to seven.

D. Lateral material distribution

With bar outer dimensions and thickness limits fixed, distribution of materials across a bar's width (along the y axis) is the most effective way to affect its torsional behavior. This is most readily observable in models 1(f), 4, and 5. Model 5 includes a locally thickened area along its center with thin areas on either side, forming a central spine. Similar features appear in other models to varying degrees. These central spines with adjacent thin areas serve to maintain vertical bending stiffness while reducing torsional and lateral bending stiffness. Such an effect is most evident in model 5 which tunes mode L1 down to a frequency ratio of six. The opposite effect is observed in model 4, which concentrates material at the bar's edges over large portions of the cutaway. This geometry increases the frequency of torsional modes, particularly mode T1. The combination of very thick edges and angled hinge segments (discussed above) in model 4 has the combined effect of raising the frequency ratio of mode T1 while lowering that of mode T2.

E. Constraint effects

Different tuning ratios may be more or less easily attained, or even infeasible, depending on a bar's note and outer dimensions. All models in this work were constrained to use measured outer dimensions from existing bars tuned to the typical 1:4:10 ratios. It stands to reason then that models 4 and 7 have some of the most unusual geometry, as frequency ratios for the three vertical bending modes in these models depart significantly from 1:4:10.

Outer bar dimensions play a key role in determining the feasibility of tuning torsional and lateral modes. Bars positioned on the lower end of a marimba keyboard, around note C2 for a five-octave marimba, tend to have long cutaways with mostly thin bar material. Such bars leave little available material with which to tune other modes. Fortunately, marimba bars with problematic torsional modes tend to be further up the keyboard. Such bars will generally provide greater flexibility in distributing material to tune torsional modes.

The effect of bar outer dimensions is also evident in the vibraphone bar models of Fig. 11. As shown in Table I, end thickness measured for the Yamaha vibraphone bar was slightly more than half that of the Adams marimba bar, while their minimum thickness values were similar. This left a smaller proportion of material for the tuning algorithm to distribute in the vibraphone bar models. With less distributable material available, the vibraphone bar models showed fewer feasible tuning ratios than the marimba bar models.

This situation is reflected in the number of models shown in Fig. 11 and the tuning ratios selected. Larger outer bar dimensions would surely increase the number of tuning ratios achievable for these aluminum bars.

Maintaining segments of uniform thickness at each end of the bar will also limit attainable frequency ratios to some extent. Previous works (Henrique and Antunes, 2003; Soares *et al.*, 2021) that allowed bar thickness to vary over the entire length were able to achieve a variety of ratios in vertical bending modes. Uniform ends were maintained in this work to provide material for pass-through support cables.

Dual symmetry imposed by the quarter-surface definition in Fig. 2 will also serve to limit feasible tuning ratios. This symmetry provided computational benefits by reducing the number of inputs. Some may also argue symmetric cutaways are aesthetically more desirable. Nevertheless, it may be interesting to explore feasible bar tuning without this imposed symmetry.

F. Strength considerations

The results presented here are intended to demonstrate tuning feasibility, not necessarily viable bar designs. Modeling of bar stresses during a mallet strike was not considered in this work. The imposed lower thickness limits in Table I are based on minimum observed thicknesses near the midpoints of existing bars. Worst-case bending stresses can be expected at these positions when mallet strikes occur in these same locations. Limiting modeled bar thickness to these minimum values should produce bars with generally comparable strength performance. However, bars with rapidly varying geometry, such as models 3, 4, and 6(b) may produce stress concentrations not present in typical bars. Fatigue could also become a concern where deformations are concentrated in small areas, as may be observed in the hinge segments described above. Any fully viable bar design must address strength considerations such as these.

G. Practical fabrication aspects

Any of the bars in Figs. 9–11 would require automated manufacturing on equipment like a CNC mill to produce such complex shapes while tuning multiple modes to precise frequencies. The natural variability of wood, both between samples and even within a sample, will complicate achieving accurate results through CNC milling. Actual wood will depart to varying extent (possibly quite significantly) from the uniform orthotropic materials used in computer models. Some work has been done exploring marimba bar fabrication via CNC mill (Mingming, 2011). Sharp edges and steep slopes observed in models 3, 4, and 6(b), may also prove impractical for wood, in light of its anisotropy and inherent heterogeneity.

As a manufactured isotropic material, aluminum lends itself more readily to CNC milling, though the process is by no means trivial. Aluminum idiophone bars produced by

CNC mill also appear in the literature (Kirkland and Moradi, 2016) with uniform thickness across their width.

Another important practical consideration is the possibility of beating if two modes designed to have the same frequency are slightly misaligned. Such a scenario could arise due to manufacturing tolerances, material variability or modeling error. This issue could occur with models 3, 5, 6(a), and 6(b) given their repeated frequency ratios.

Considering these practical aspects, model 2 is likely the most viable candidate for fabrication amongst the marimba bar models. This model tunes the frequency ratio of mode T2 one integer multiple higher than that of mode V3, while leaving modes T1 and L1 untuned. Model 2 is thus intended to separate the frequencies of modes V3 and T2 while departing only mildly from typical cutaway geometry.

H. Mode participation

A common question in discussing this work is: “what are the relative magnitudes of these modes in the bar’s response?” The answer depends on several factors. The most important factor is strike location and direction. If the bar is struck at a point where a mode has significant displacement along the direction of the strike, that mode will be excited. Bars are typically struck perpendicular to the playing surface with motion predominantly in the z -direction. Figure 4 shows a bar with color map corresponding to the fundamental mode shape. A mallet strike in a red area in Fig. 4 would produce maximum participation of this mode, whereas a strike in a blue area would produce minimum participation. A second factor in modal participation is radiation efficiency. In the first torsional mode, shown in Fig. 1(T), the mode shape is anti-symmetric about the bar’s centerline (along the x axis). On either side of the centerline the motion of this mode is 180° out of phase. Thus, it is not expected that this mode would contribute significantly to the bar’s far-field response. Support conditions on a real instrument and the presence of resonator tubes would also affect sound radiation from each mode. These considerations provide some interesting avenues for future investigation.

I. Algorithm performance

The algorithm outlined in Sec. III successfully tuned bars to the frequency ratios in Table III as well as numerous others. Not all frequency ratios were achievable using the model, constraints and tuning approach described in Sec. III. If an analysis did not converge after a specified maximum number of iterations, its target frequency ratios were deemed infeasible within this framework.

As expected, the algorithm identified geometries that tuned the specified modes while prioritizing similarity to the given initial geometry. This is evident in models 6(a) and 6(b) as well as model 10. Though only vertical modes are tuned in model 10, it can be shown that the final input vector for model 10 is closer to its initial input vector than if thickness had remained constant across the bar’s width (as is the

case in the initial carved geometry). This results from interior control points exerting greater influence on tuning than control points on the bar’s edge.

Convergence rates were observed to slow down as the control point thickness inputs began reaching one of the thickness limits in Table I. The binary matrix added in Eq. (6) improved convergence in these cases. Further improvement was achieved by setting control point thickness values in the initial geometry (see Fig. 3) near the lower limit. With many thickness inputs beginning near the lower limit, these values tended to move away from that limit during tuning rather than toward it. This approach also improved convergence rates, with the caveat that thin initial cutaway geometries will lead to relatively thin final geometries.

The mode identification methods outlined in Sec. IV generally performed well, though some issues were noted identifying lateral modes in the relatively thin vibraphone bars.

VI. CONCLUDING REMARKS

This work has demonstrated the feasibility of tuning marimba and vibraphone bar vertical, lateral, and torsional modes using cutaway shapes that vary along the bar’s length and width. No concentrated masses or additional materials were employed. The resulting bar shapes are complex and would require automated milling to produce. The Newton-Raphson method, applied to an underdetermined system using the Moore-Penrose inverse, performed well in tuning feasible frequency ratios while favoring bar shapes similar to initial geometries. This approach provides the efficiency benefits of gradient-based tuning, while allowing a number of input variables greater than the number of tuned modes. The surface interpolation employed provides great flexibility in defining bar cutaway geometry while maintaining a manageable number of inputs for the tuning procedure. Methods were implemented to automatically identify mode shapes, even in the presence of degenerate modes. This ability is a necessary ingredient for any algorithm seeking to tune specific 3D modes without the need for human intervention.

The resulting bar geometries represent interesting new shapes with varying degrees of viability for bar design. While numerous frequency ratios were successfully tuned, using even harmonics, odd harmonics, or a mixture, not all ratios were possible with the constraints and methods employed. In some cases, achieving a desired set of frequency ratios may require relaxing symmetry constraints and increasing the number of geometry control points, forgoing sections of uniform thickness at bar ends, or adjusting overall bar dimensions or materials. There are, of course, some frequency ratios that may never be possible due to practical limitations of bar dimensions and material properties.

These results raise interesting questions. To what extent will such tuned torsional modes be audible, depending on mallet strike location? What frequency ratios for these

modes would be preferable for performers and listeners? Could such modes be used to create noticeably variable bar timbre depending on strike location? How will the performance of fabricated bars compare with predicted model results? Such questions provide potential avenues for future research.

ACKNOWLEDGEMENTS

This research was supported by the Vanier Canada Graduate Scholarships program. The authors would also like to thank Mr. Darryl Cameron for assistance with computing resources and Mr. Martin Daigle for providing access to instruments.

Allemang, R. J. (2003). "The modal assurance criterion—Twenty years of use and abuse," *Sound Vib.* **37**(8), 14–21.

Battelle Memorial Institute (2020). *Metallic Materials Properties Development and Standardization (MMPDS-15)* (Battelle Memorial Institute, Columbus, OH), Chap. 3.

Beaton, D., and Scavone, G. (2019). "Optimization of marimba bar geometry by 3D finite element analysis," in *Proceedings of International Symposium on Musical Acoustics 2019*, Detmold, pp. 402–407.

Ben-Israel, A. (2002). "The Moore of the Moore-Penrose inverse," *Electron. J. Linear Algebra* **9**, 150–157.

Ben-Israel, A., and Greville, T. N. E. (2003). *Generalized Inverses: Theory and Applications*, 2nd ed. (Springer, New York), pp. 109–110.

Bestle, P., Eberhard, P., and Hanss, M. (2017). "Musical instruments—Sound synthesis of virtual idiophones," *J. Sound Vib.* **395**, 187–200.

Bork, I., Chaigne, A., Trebuchet, L.-C., Kosfelder, M., and Pillot, D. (1999). "Comparison between modal analysis and finite element modeling of a marimba bar," *Acta Acust. Acust.* **85**(2), 258–266.

Bretos, J., Santamaría, C., and Moral, J. A. (1997). "Tuning process of xylophone and marimba bars analyzed by finite element modeling and experimental measurements," *J. Acoust. Soc. Am.* **102**(6), 3815–3816.

Bretos, J., Santamaría, C., and Moral, J. A. (1999). "Finite element analysis and experimental measurements of natural eigenmodes and random responses of wooden bars used in musical instruments," *Appl. Acoust.* **56**(3), 141–156.

Chaigne, A., and Doutaut, V. (1997). "Numerical simulations of xylophones. I. Time-domain modeling of the vibrating bars," *J. Acoust. Soc. Am.* **101**(1), 539–557.

Dhondt, G. (2019). "CalculiX: A three-dimensional structural finite element program" <http://www.calculix.de> (Last viewed April 14, 2021).

Henrique, L. L., and Antunes, J. (2003). "Optimal design and physical modelling of mallet percussion instruments," *Acta Acust. Acust.* **89**(6), 948–963.

Kanzow, C., Yamashita, N., and Fukushima, M. (2004). "Levenberg-Marquardt methods with strong local convergence properties for solving nonlinear equations with convex constraints," *J. Comput. Appl. Math.* **172**(2), 375–397.

Kirkland, W. B., and Moradi, L. (2016). "Topographical optimization of structures for use in vibraphones and other applications," in *Proceedings of the Society for Design and Process Science 21st International Conference*, Orlando, FL, pp. 69–77.

Macconi, M., Morini, B., and Porcelli, M. (2009). "A Gauss-Newton method for solving bound-constrained underdetermined nonlinear systems," *Optim. Meth. Softw.* **24**(2), 219–235.

Mingming, Z. (2011). "Automatic multi-modal tuning of idiophone bars," Master's thesis, Curtin University, Perth, Australia.

Moore, J. L. (1970). "Acoustics of bar percussion instruments," Ph.D. thesis, The Ohio State University, Columbus, OH.

Orduña-Bustamante, F. (1991). "Nonuniform beams with harmonically related overtones for use in percussion instruments," *J. Acoust. Soc. Am.* **90**(6), 2935–2941.

Penrose, R. (1955). "A generalized inverse for matrices," *Math. Proc. Cambridge Philos. Soc.* **51**(3), 406–413.

Petrolito, J., and Legge, K. A. (1997). "Optimal undercuts for the tuning of percussive beams," *J. Acoust. Soc. Am.* **102**(4), 2432–2437.

Petrolito, J., and Legge, K. A. (2005). "Designing musical structures using a constrained optimization approach," *J. Acoust. Soc. Am.* **117**(1), 384–390.

Soares, F., Antunes, J., and Debut, V. (2021). "Multi-modal tuning of vibrating bars with simplified undercuts using an evolutionary optimization algorithm," *Appl. Acoust.* **173**, 107704.

Stevens, L. H. (2015). "The acoustic complexity of keyboard percussion instruments. Part I: What we know and what we wish we knew," *J. Acoust. Soc. Am.* **138**(3), 1912.

Wang, S.-Y., Sun, Y., and Gallagher, R. (1985). "Sensitivity analysis in shape optimization of continuum structures," *Comput. Struct.* **20**(5), 855–867.